

# Skipping orbits and enhanced resistivity in large-diameter InAs/GaSb antidot lattices

J. Eroms\*, M. Zitzlsperger, D. Weiss

*Universität Regensburg, D-93040 Regensburg, Germany,*

J. H. Smet, C. Albrecht

*Max-Planck-Institut für Festkörperforschung, Heisenbergstraße 1, D-70569 Stuttgart, Germany*

R. Fleischmann

*Max-Planck-Institut für Strömungsforschung, Bunsenstr. 10, D-37073 Göttingen, Germany*

M. Behet, J. De Boeck, G. Borghs

*IMEC, Kapeldreef 75, B-3001 Leuven, Belgium*

We investigated the magnetotransport properties of high mobility InAs/GaSb antidot lattices. In addition to the usual commensurability features at low magnetic fields we found a broad maximum of classical origin around 2.5 T. The latter can be ascribed to a class of rosetta type orbits encircling a single antidot. This is shown by both a simple transport calculation based on a ‘classical’ Kubo formula and an analysis of the Poincaré surface of section at different magnetic field values. At low temperatures we observe weak  $1/B$ -periodic oscillations superimposed on the classical maximum.

(April 26, 2018)

Periodically modulated two-dimensional electron gases (2DEGs) offer the possibility to study electron motion in artificially tailored periodic potentials.<sup>1</sup> If the modulation potential is strong enough to deplete parts of the 2DEG around the potential maxima the system is called an antidot (AD) array. Antidot lattices are model systems to study both the classical chaotic motion of electrons in the potential landscape as well as resulting bandstructure effects.<sup>1</sup> Investigations so far have essentially focused on the low field regime where the low-temperature magnetoresistance reflects peaks whenever the classical cyclotron diameter  $2R_c$  fits around a (geometry-dependent) specific number of antidots.<sup>2</sup> The last maximum appears in the resistivity when  $2R_c$  is equal to the period  $a$  of the array. Here we focus on novel structure appearing at slightly higher fields corresponding to  $B$ -values where  $2R_c < a$  holds. While antidot lattices are usually based on GaAs/AlGaAs heterojunctions, we used here the material system InAs/GaSb to fabricate antidot arrays. Due to the pinning of the Fermi energy within the conduction band at open surfaces of InAs,<sup>3</sup> depletion regions around the antidots should be significantly smaller than in GaAs based systems. This should allow, due to the resulting steep potential posts, to fabricate very short period antidot arrays or, as it is the case here, the fabrication of large antidots with small constrictions between neighboring antidots.

Our samples are fabricated from InAs/GaSb heterostructures grown on undoped GaAs substrates by molecular beam epitaxy. The epitaxial layers on the substrate consist of a  $1.1 \mu\text{m}$  AlGaSb layer, a  $0.5 \mu\text{m}$  thick

GaSb buffer followed by a ten period AlSb/GaSb superlattice, the GaSb barrier of 50 nm thickness, the 15 nm InAs quantum well and a 5 nm GaSb top layer (see upper inset in Fig. 1). While the heterostructure is nominally undoped, the carrier concentration  $n_s$  can be adjusted by the top layer thickness.<sup>4-6</sup> Typical values of  $n_s$  in our unpatterned samples were about  $1.5 \cdot 10^{12} \text{cm}^{-2}$ . Hallbars were defined by standard photolithography and wet chemical etching.<sup>7</sup> It turned out that the alkaline photoresist developer attacks the GaSb-layer and decreases the carrier mobility from about  $400\,000 \text{cm}^2/\text{Vs}$  to about  $100\,000 \text{cm}^2/\text{Vs}$ . An annealing step at  $270^\circ\text{C}$  in a continuous flow of forming gas restored the mobility to about  $300\,000 \text{cm}^2/\text{Vs}$ . This corresponds to a mean free path of  $6 \mu\text{m}$  which is much larger than the lattice period  $a = 380 \text{nm}$ , thus making commensurability features observable. Since InAs does not form a Schottky barrier to metals, it was not necessary to use alloyed contacts. Instead of gold, which proved to react with GaSb in the final annealing step, we used evaporated indium contacts. The antidots were defined with electron beam lithography and etched with the solution described above. A scanning electron micrograph of the samples showed the antidots to be uniform in size and shape with an AD diameter of 250 nm.

The four-point magnetotransport measurements were carried out at temperatures ranging from 1.5 K to 40 K using standard lock-in techniques. Utilising the negative persistent photo-conductivity of InAs quantum wells,<sup>8</sup> the carrier density could be varied by illuminating the sample with a red LED. The magnetoresistance and Hall

resistance traces at a carrier density of  $1.33 \cdot 10^{12} \text{ cm}^{-2}$  and a temperature of 1.5 K are shown in Fig. 1. At low fields two commensurability peaks in the magnetoresistance curve can be observed. The peak at about 1 T belongs to trajectories going around one antidot, the other one at 0.25 T corresponds to a deformed cyclotron orbit around four antidots. In the simplest model, the enhanced resistivity at these field values can be ascribed to electrons pinned on commensurate cyclotron orbits, which cannot carry current.<sup>2,10</sup> At fields above 3.5 T strong Shubnikov-de Haas (SdH) oscillations appear and from 6 T spin-splitting of the Landau levels is resolved. By comparison to an unpatterned reference sample, we can conclude that the quality of the 2DEG was not seriously affected by the patterning process. In the region between 1.5 T and 3.5 T we find a new broad peak structure whose origin will be discussed below. In earlier work, a corresponding shoulder was ascribed to etch-induced defects.<sup>9</sup> For a sample with triangular antidots, a high-field shoulder at  $2R_c = a/2$  was explained by electrons being reflected on the straight antidot edges.<sup>11</sup>

Figure 2 shows the dependence of the magnetoresistance traces on the carrier density (changed by illumination) and temperature (inset). The novel peak structure shifts similar to the main commensurability maximum at  $2R_c = a$ . This suggests, together with the weak temperature dependence of the peaks (see lower inset of Fig. 2), a classical origin of the phenomenon. Associating the magnetic field value at which the broad maxima start to appear (marked by arrows) with the matching condition  $R_c = b$  we find a value of  $b = 110 \text{ nm}$ . This value  $b$  corresponds to the distance between neighboring antidots in our device. This finding is consistent with the assumption that the broad maximum is associated with rosetta shaped orbits skipping around one antidot, as we will show below.

Superimposed on the classical peak we find  $1/B$ -periodic quantum oscillations. While the periodicity of these oscillations is similar to the period of the SdH-oscillations at higher magnetic field, there is a distinct transition between the high-field oscillations and the ones superimposed upon the classical maximum. This can be seen in the upper inset of Fig. 2 where the filling factor  $\nu$  is plotted versus  $1/B$ . At around 4 T there is a pronounced kink in the otherwise linear slope which is observed at the transition between the classical peak regime and the quantum mechanical regime in which Shubnikov-de Haas oscillations dominate. Compared to the Shubnikov-de Haas oscillations the amplitude of oscillations superimposed upon the classical peak structure is strongly suppressed. We speculate that the weak  $1/B$ -periodic oscillations in the low field regime stem from quantization of the skipping orbits. The quantum oscillations are suppressed at temperatures above a few Kelvin (see lower inset of Fig. 2) while the classical features survive up to temperatures of 40 K where they are blurred as the GaSb substrate becomes conducting.

In order to clarify the origin of the classical maximum

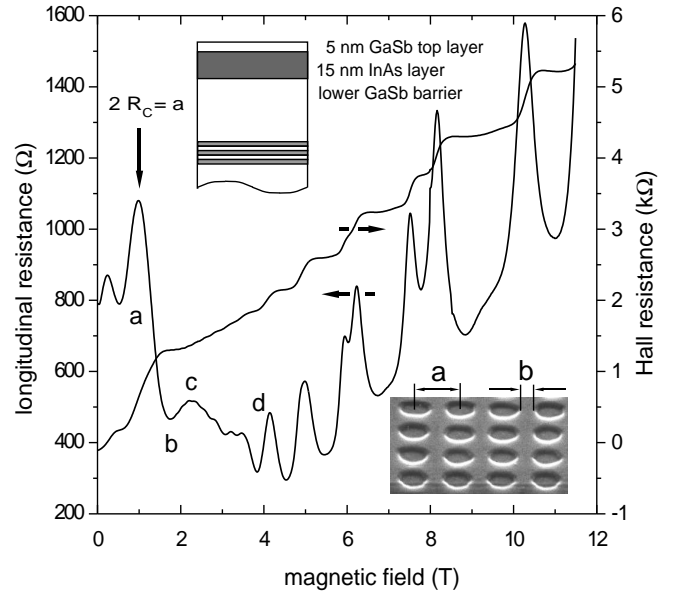


FIG. 1. Magnetoresistance and Hall resistance of an InAs/GaSb antidot lattice. Lower inset: A SEM picture of the sample. Upper inset: Layer sequence of the heterostructure as described in the text. Letters a to d denote  $B$ -field positions of interest, which are analysed numerically in Fig. 4.

between 1.5 T and 3.5 T we carried out numerical calculations following recent work.<sup>10</sup> We evaluated the Kubo formula<sup>12</sup>

$$\sigma_{ij} = \frac{e^2 m^*}{\pi \hbar^2} \int_0^\infty dt e^{-t/\tau} \langle v_i(t) v_j(0) \rangle$$

to calculate the conductivity tensor  $\sigma_{ij}$  where the indices  $i$  and  $j$  stand for the  $x$ - and  $y$ -direction. The trajectories and the resulting velocities  $v_i$  and  $v_j$  were calculated numerically assuming a hard wall potential. The brackets denote the average over phase space. Previously only chaotic trajectories were considered in the evaluation of the Kubo formula.<sup>10</sup> Since the features we are interested in appear at relatively high magnetic field values, most of the phase space is occupied by regular non-chaotic trajectories. Therefore we included both regular and chaotic trajectories in our calculations. By inverting the conductivity tensor we obtain the experimentally determined diagonal resistivity  $\rho_{xx}$ . The results of a simulation using the simple model with perfectly hard walls are shown in Fig. 3. The calculated traces are remarkably close to the experimental results: the additional structure between 1.5 and 3.5 T was nicely reproduced.<sup>13</sup>

To obtain information about the types of trajectories involved in the observed magnetoresistance anomalies we analysed the Poincaré surfaces of section at different magnetic field values. This is done by injecting electrons at  $x = 0$  (between two antidots; see left hand side of the lower inset of Fig. 4) with velocity  $v_y$  into the lattice and recording the  $v_y$  and  $y$  values of the injected electrons intersecting the line  $x \bmod a = 0$ . To take into account

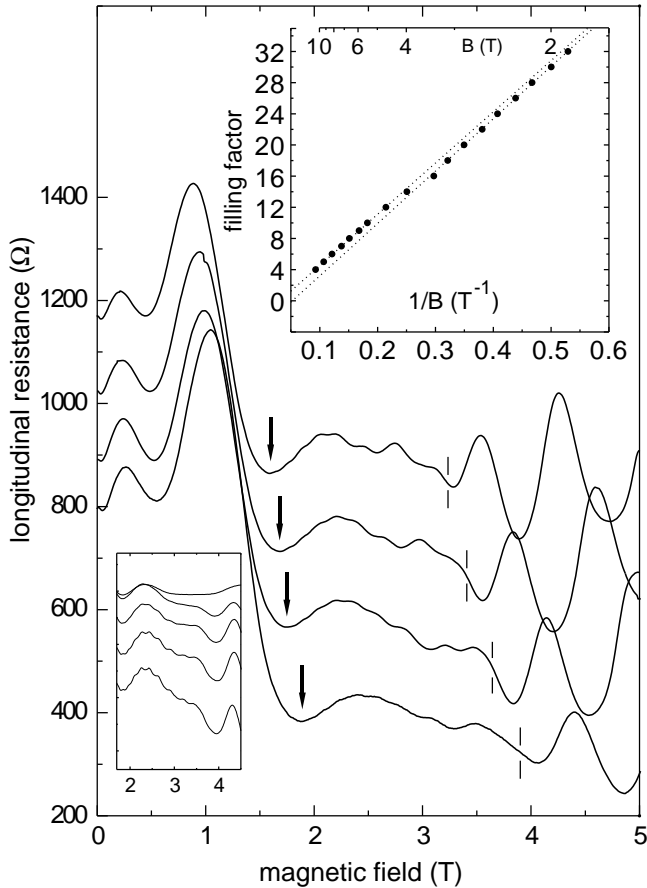


FIG. 2. Density dependence of the magnetoresistance. Electron densities (from top to bottom):  $1.13 \cdot 10^{12} \text{ cm}^{-2}$ ,  $1.24 \cdot 10^{12} \text{ cm}^{-2}$ ,  $1.33 \cdot 10^{12} \text{ cm}^{-2}$ , and  $1.42 \cdot 10^{12} \text{ cm}^{-2}$ . Arrows indicate the beginning of the new structure, vertical lines mark the onset of strong SdH oscillations. Lower inset: Temperature dependence of the features at  $n_s = 1.42 \cdot 10^{12} \text{ cm}^{-2}$ . Temperatures are 1.5 K, 3 K, 10 K, 20 K, and 40 K from bottom to top. Graphs are offset by  $100 \Omega$  for clarity. Upper inset:  $1/B$ -position of the minima of the quantum oscillations. Filling factors  $\nu$  correspond to the carrier density determined at high fields. A magnetic field axis is included for guidance.

possible soft wall effects we assumed here an antidot potential of the form

$$V(x, y) = V_0 \left( \cos \frac{\pi x}{a} \cdot \cos \frac{\pi y}{a} \right)^\beta$$

with  $\beta = 16$ . The trajectories and velocities of the injected electrons were obtained by solving the classical equations of motion numerically at several magnetic fields (indicated with letters a to d in Figs. 1 and 4).

At about 1 T (letter a), the commensurability condition  $2R_c = a$  is satisfied, and the Poincaré surface of section exhibits a stable island in Fig. 4a belonging to cyclotron orbits around one antidot. This leads to the fundamental commensurability peak in  $\rho_{xx}$ . The minimum in the magnetoresistance at 1.9 T (letter b) is due to the fact that the large antidots leave no room for sta-

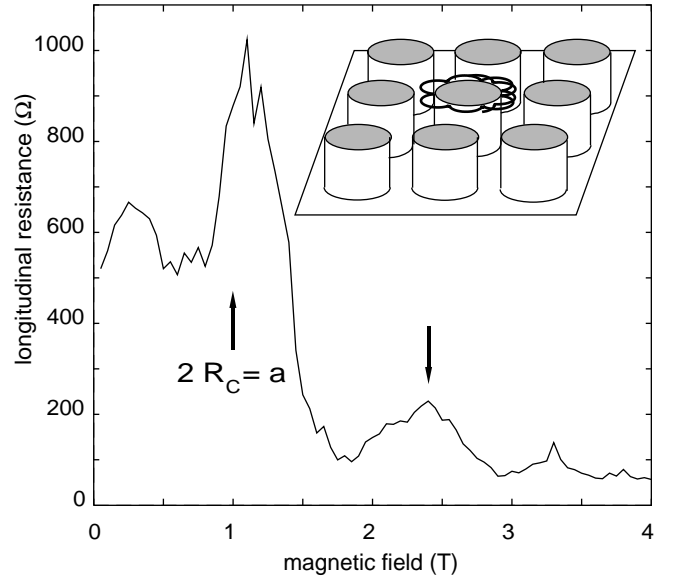


FIG. 3. Magnetoresistance traces obtained with a simple simulation based on the Kubo formula. The commensurability condition  $2R_c = a$  is shown for  $n_s = 1.3 \cdot 10^{12} \text{ cm}^{-2}$  used in the calculation. Inset: A sketch of the hard-wall potential and a rosetta orbit encircling an antidot. Its magnetic field position is marked with an arrow in the large graph.

ble trajectories. This minimum is not found in antidot lattices with smaller AD diameters. If the magnetic field gets higher, the Poincaré surface of section c shows that a large fraction of phase space is occupied by periodic and quasi-periodic trajectories. These are rosetta shaped orbits, which encircle one antidot and remain stationary even if an electric field is applied in the simulation, giving rise to a maximum in the magnetoresistance at 2.5 T. The situation is quite similar to pinned orbits, which are responsible for the commensurability peak at  $2R_c = a$ . The high field behaviour (letter d,  $B = 4 \text{ T}$ ) of the classical structure is governed by the formation of unstable rosetta orbits. Instead of being composed more or less of semicircles, the small cyclotron diameter at high fields permits orbits which resemble circles revolving around one antidot. These orbits tend to drift perpendicular to an electric field, thus reducing  $\rho_{xx}$ , even though the stable orbits still occupy a large volume in phase space.

When the magnetic field exceeds 3.5 T, the amplitude of the SdH-oscillations increases drastically. At lower fields the cyclotron diameter exceeds the width of the constriction between adjacent antidots. Therefore, electrons can move easily from one edge of the sample to the other by hopping from AD to AD. As soon as the cyclotron diameter becomes smaller, this backscattering process is no longer possible and the SdH-oscillations become much more pronounced. From the magnetic field position of this point we determine this critical cyclotron diameter to be 110 nm. If we assume a very steep antidot potential, this leads to an antidot diameter of 270 nm which is a little larger than the lithographic diameter of

